

Article

# Influence of Ti Content on the Partial Oxidation of $\text{Ti}_x\text{FeCoNi}$ Thin Films in Vacuum Annealing

Ya-Chu Yang <sup>1</sup>, Jien-Wei Yeh <sup>1,\*</sup> and Chun-Huei Tsau <sup>2,\*</sup>

<sup>1</sup> Department of Materials Science and Engineering, National Tsing Hua University, Hsinchu 300, Taiwan; yachu.y@gmail.com

<sup>2</sup> Institute of Nanomaterials, Chinese Culture University, Taipei 111, Taiwan

\* Correspondence: jwyeh@mx.nthu.edu.tw (J.-W.Y.); chtsau@staff.pccu.edu.tw (C.-H.T.); Tel.: +886-3-571-9558 (J.-W.Y.); +886-3-582-6140 (C.-H.T.)

Received: 5 August 2017; Accepted: 25 September 2017; Published: 27 September 2017

**Abstract:** This study investigated the effects of Ti content and vacuum annealing on the microstructure evolution of  $\text{Ti}_x\text{FeCoNi}$  ( $x = 0, 0.5, \text{ and } 1$ ) thin films and the underlying mechanisms. The as-deposited thin film transformed from an FCC (face center cubic) structure at  $x = 0$  into an amorphous structure at  $x = 1$ , which can be explained by determining topological instability and a hard ball model. After annealing was performed at 1000 °C for 30 min, the films presented a layered structure comprising metal solid solutions and oxygen-deficient oxides, which can be major attributed to oxygen traces in the vacuum furnace. Different Ti contents provided various phase separation and layered structures. The underlying mechanism is mainly related to the competition among possible oxides in terms of free energy production at 1000 °C.

**Keywords:** sputtering; vacuum annealing; oxide; thin films

## 1. Introduction

A very low resistivity (30  $\mu\Omega\cdot\text{cm}$ ) of the  $\text{TiFeCoNiO}_x$  thin film is observed in our previous study [1], and it is observed during the test of oxidation resistance of the thin films. This phenomenon is caused by the different activities with oxygen, Ti has higher affinity with oxygen than the other elements. Therefore, Ti migrates to the surface and forms a TiO-rich oxide, the other elements form a FeCoNi-rich alloy which provides a very good conductivity. A similar phenomenon is also observed in  $\text{AlFeCoNiO}_x$  oxide film, because aluminum also has a very high affinity with oxygen [2]. However, the resistivity of  $\text{CrFeCoNiO}_x$  oxide film is not as low as the oxide films of  $\text{TiFeCoNiO}_x$  and  $\text{AlFeCoNiO}_x$  because of its activity with oxygen. Also, the lowest resistivity of every oxide film is achieved after 1000 °C for 30 min vacuum annealing; after that, the resistivity increases with increasing the annealing time. This decreasing of resistivity of these thin films contributes to the recrystallization and deficient oxidation. This phenomenon is very interesting for academic research.

The parent study investigated the phase transformations and deficient oxides through vacuum annealing. The mechanism of partial oxidation is an important factor to understand the origin of low resistivity. In this study, thin films with various quantities of Ti, such as  $\text{Ti}_x\text{FeCoNi}$  ( $x = 0, 0.5, 1.0$ ), were designed and prepared through sputter deposition and subsequent vacuum annealing to reveal the mechanism of the partial oxidation of  $\text{Ti}_x\text{FeCoNi}$  film during vacuum annealing.

## 2. Experimental Procedures

FeCoNi (designated as  $\text{Ti}_0$ ),  $\text{Ti}_{0.5}\text{FeCoNi}$  ( $\text{Ti}_{0.5}$ ), and  $\text{TiFeCoNi}$  ( $\text{Ti}_{1.0}$ ) alloy targets with a diameter of 2 inches were prepared from high-purity Ti, Fe, Co, and Ni via vacuum arc melting and machining. The chemical compositions of the  $\text{Ti}_x\text{FeCoNi}$  targets listed in Table 1 were determined using an energy

dispersive spectrometer (EDS) of a field emission scanning electron microscope (SEM, JEOL JSM-6335, JEOL Ltd., Tokyo, Japan) operated at 15 kV. The substrate used for deposition was a SiO<sub>2</sub>/Si wafer, whose 0.3 μm thick SiO<sub>2</sub> layer was formed by heat treatment at 1000 °C for 24 h. The SiO<sub>2</sub> layer served as a barrier to prevent the diffusion of Si from the substrate to the film during high-temperature annealing. Ti<sub>x</sub>FeCoNi thin films were deposited on the SiO<sub>2</sub>/Si substrates by using a direct current (DC) sputtering system, without bias and temperature control. The substrates were placed approximately 11 cm from the target on the center of a substrate table which was rotated at a speed of 5 rpm. Prior to deposition, both the substrate and target were independently sputter cleaned by means of a shutter placed between them. It was performed at 100 W and the flow rate of Ar was 30 standard cubic centimeter per min (sccm). The background and working pressures were  $5 \times 10^{-5}$  and  $2 \times 10^{-3}$  torr, respectively. The deposition power was 100 W and the deposition rate was 133 Å/min. Some of the deposited samples were further annealed in a vacuum tube furnace at 1000 °C for 30 min.

**Table 1.** Chemical compositions of the Ti<sub>x</sub>FeCoNi targets analyzed by SEM/EDS.

Targets	Compositions (at %)			
	Ti	Fe	Co	Ni
Ti <sub>0</sub>	-	32	34	34
Ti <sub>0.5</sub>	12	28	30	30
Ti <sub>1</sub>	23	25	26	26

The crystallographic structures of the Ti<sub>x</sub>FeCoNi films were examined using glancing angle incidence (2°) X-ray diffractometer (XRD, Rigaku TTRAX III, Rigaku Ltd., Tokyo, Japan) with Cu Kα<sub>1</sub> radiation ( $\lambda = 0.15406$  nm) generated at 50 kV and 300 mA. The microstructures and compositions of the thin films were further investigated in detail by utilizing a field emission transmission electron microscope (TEM, FEI Tecnai S-Twin, Thermo Fisher Scientific, Waltham, MA, USA) equipped with an EDS.

### 3. Results and Discussion

Figure 1a,b show the typical cross-section SEM images of as-deposited and as-annealed Ti<sub>x</sub>FeCoNi thin films, respectively. All of these three alloy thin films had a similar micrograph under as-deposited or as-annealed state. The as-deposited thin film has a columnar structure, shown in Figure 1a. However, each single column was not a single grain. TEM observation described below proved that the FeCoNi alloy thin film had a nano-grained structure. This nano-grained structure would become an amorphous structure after the Ti-content increased; the TiFeCoNi alloy thin film thus had a fully amorphous structure. The microstructures of these thin films become to a coarse-grained one after vacuum annealing at 1000 °C for 30 min, shown in Figure 1b; and different phases were formed after annealing because of diffusion of atoms and oxidation.

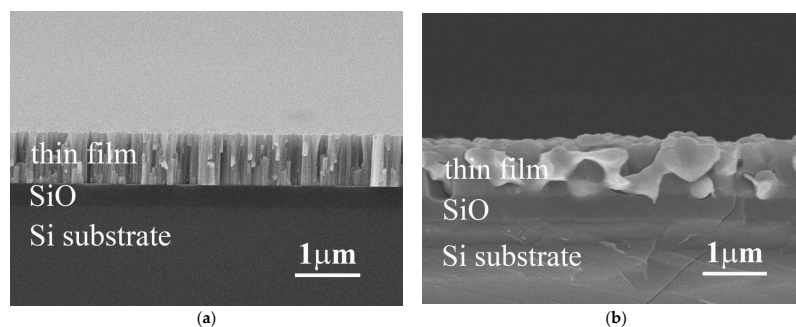


**Figure 1.** The typical SEM micrographs of (a) the as-deposited Ti<sub>0</sub> thin film; and (b) the as-annealed Ti<sub>0.5</sub> thin film.

Figure 2 presents the XRD patterns and the crystallographic structures of  $Ti_xFeCoNi$  thin films in as-deposited and as-annealed states. The FCC peaks indicate that the as-deposited  $Ti_0$  and  $Ti_{0.5}$  films present a single FCC structure with a nano-crystalline structure, which is confirmed in the latter section of the TEM analysis; while the broad peak shows that the  $Ti_{1.0}$  film has an amorphous structure. The formation of an FCC structure through the as-deposited  $Ti_0$  film is reasonable because Fe, Co, and Ni atoms can substitute one another due to their similar atomic sizes, valences, and electronegativities [3]. Intensity decreases with Ti content because of the large atomic size of Ti. Thus, large lattice distortion and subsequent diffuse scattering are induced. An increase in the half-height width of the main FCC peak corresponds to a decrease in grain size that can be attributed to the reduced atom migration and grain growth when large Ti atoms are incorporated. The amorphous structure of the  $Ti_{1.0}$  film can be explained by the hard ball model proposed by Kao et al. [4]. The radii of Fe, Co, Ni, and Ti are 1.27, 1.25, 1.25, and 1.46 Å, respectively [3]. The average atomic radius of  $Ti_{1.0}$  is 1.3075 Å, and the atomic size fluctuation is between +11.7% and −4.4%. An amorphous structure is expected because the low size fluctuation of −4.4% does not satisfy the least size deviation requirement of  $\pm 7.2\%$  for the merging of the second and third atomic shells for a short-range-order amorphous structure and  $\pm 6.2\%$  for the merging of the fourth and fifth shells for a medium-range-order amorphous one. Table 2 lists the chemical compositions of the as-deposited thin films analyzed by SEM/EDS. Also all of the as-deposited thin films contained 7–8 at % oxygen which was from the deposition process.

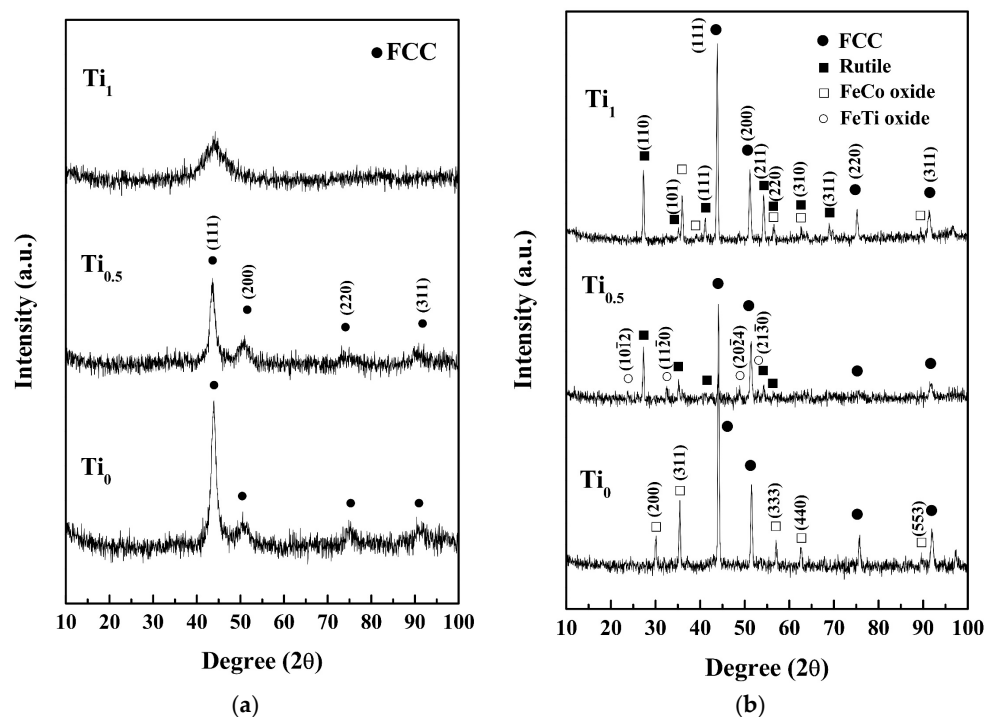


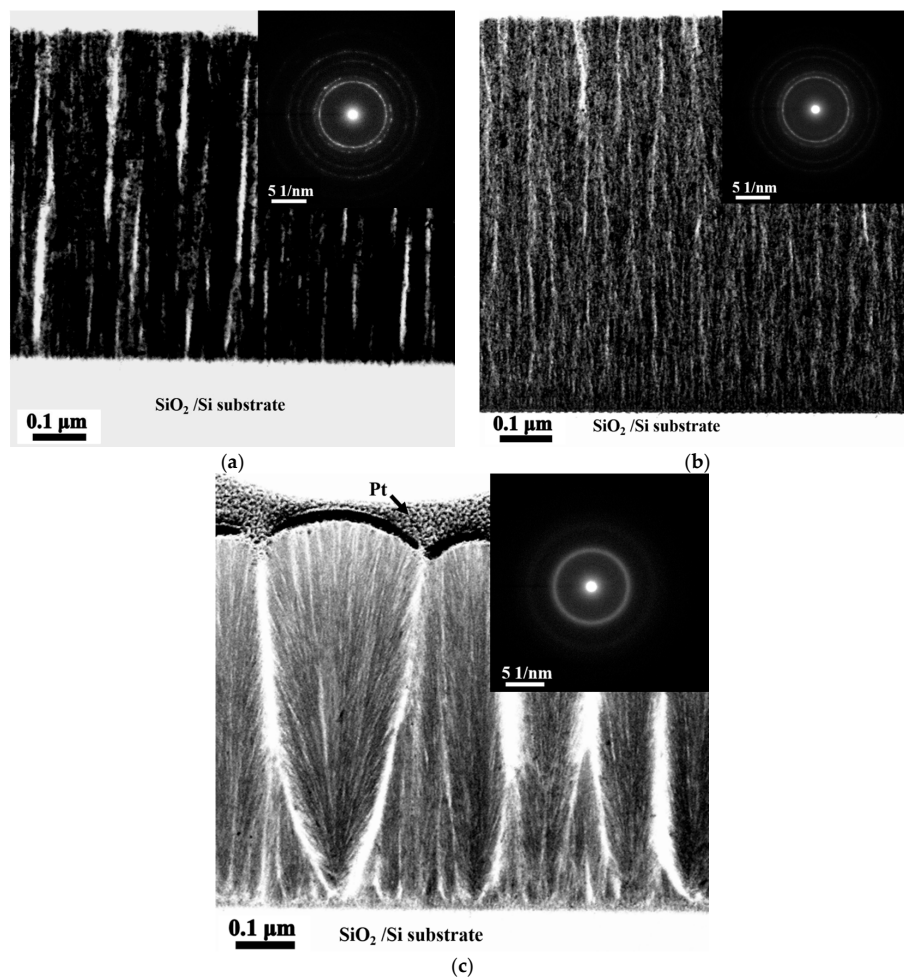
Figure 2. Glancing incident angle XRD patterns of (a) as-deposited; and (b) as-annealed  $Ti_xFeCoNi$  films.

Table 2. Chemical compositions of as-deposited  $Ti_xFeCoNi$  thin films (SEM/EDS).

Thin Film	Composition (at %)				
	O	Ti	Fe	Co	Ni
$Ti_0$	$7 \pm 1$	-	$27 \pm 2$	$33 \pm 1$	$32 \pm 1$
$Ti_{0.5}$	$7 \pm 1$	$11 \pm 1$	$25 \pm 1$	$30 \pm 1$	$27 \pm 1$
$Ti_1$	$9 \pm 1$	$22 \pm 1$	$23 \pm 1$	$25 \pm 1$	$21 \pm 1$

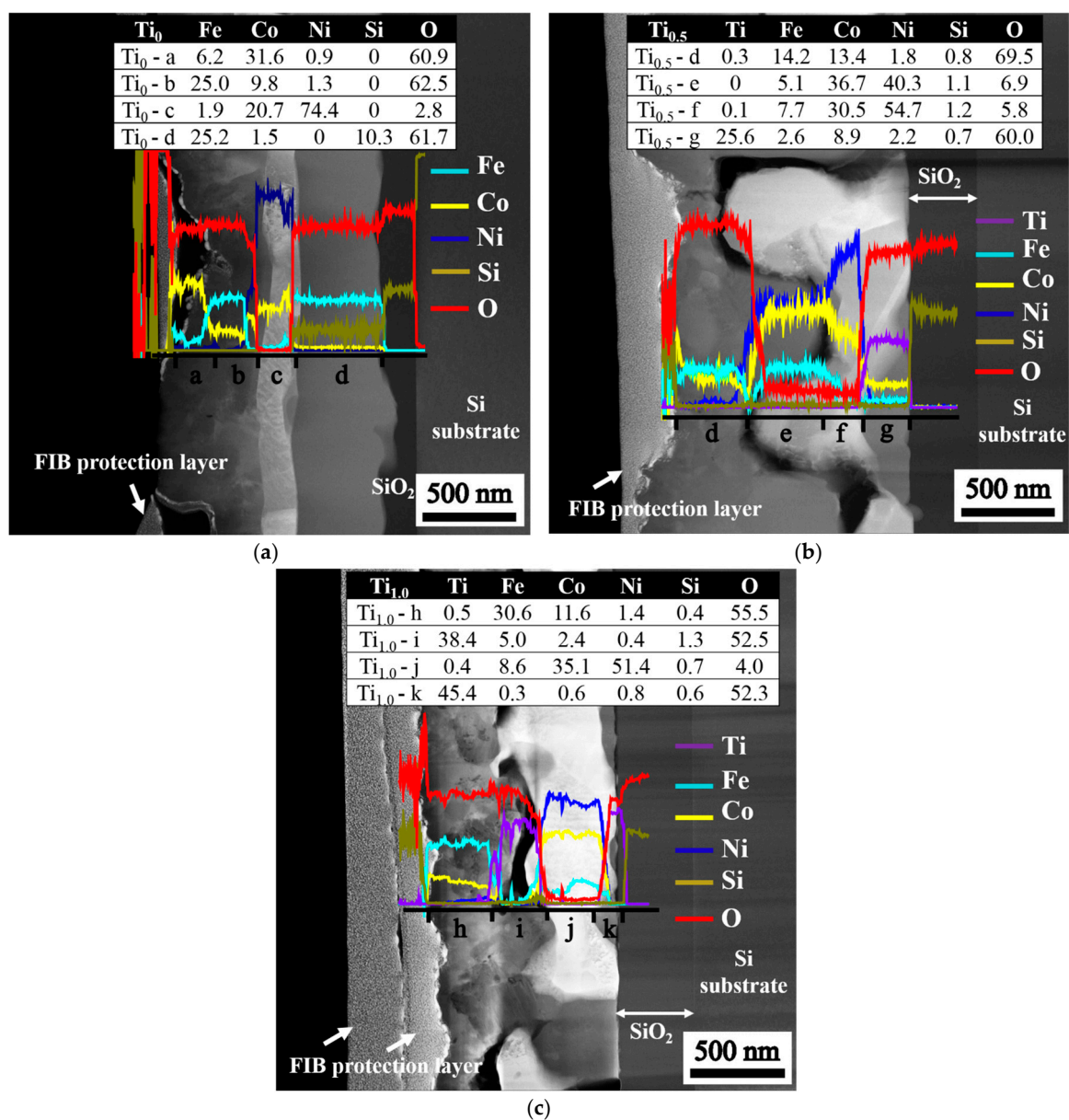
Figure 2b reveals new diffraction peaks in the XRD patterns of the films subjected to vacuum annealing. The  $Ti_0$  film presents the FeCoNi peaks and FeCo-rich oxide peaks that correspond to the FCC structures with lattice constants of 3.55 and 8.38 Å, respectively. The  $Ti_{0.5}$  film yields FeCoNi-rich, rutile- $TiO_x$ , and FeTi-rich oxide peaks. FeCoNi-rich peaks show an FCC structure with a lattice constant of 3.59 Å. Rutile peaks have a  $TiO_x$  structure (JCPDS: 76-0321) with lattice constants of  $a = 4.59$  Å and  $c = 2.95$  Å. FeTi-rich oxide peaks have a HCP structure with lattice constants of  $a = 5.09$  Å and  $c = 14.06$  Å, which are similar to  $FeTiO_3$  (JCPDS: 79-1838). The  $Ti_{1.0}$  film presents FeCoNi-rich, FeCo-rich oxide, and rutile peaks. The FeCoNi-rich and FeCo-rich oxide peaks indicate an FCC structure with lattice constants of 3.57 and 8.75 Å, respectively. However, the rutile peaks correspond to the  $TiO_x$  structure (JCPDS: 76-0321) with lattice constants of  $a = 4.609$  Å and  $c = 2.963$  Å. Overall, the as-annealed thin films retained an FCC and FeCoNi-based metal phase and formed oxides.

Figure 3a–c present the TEM bright field (BF) images and the corresponding selection area diffraction patterns (SAD) of the cross-sectional microstructures of the as-deposited  $Ti_0$ ,  $Ti_{0.5}$ , and  $Ti_{1.0}$  thin films with a columnar structure and void striations (white area) along the column boundaries [5]. The voids were unavoidable because of the shadow effect associated with oblique deposition at room temperature and without an applied bias voltage. Without atom mobility and ion bombardment enhanced by high temperature and bias bombardment, eliminating the formation of voids during deposition is difficult. Additionally, the ring patterns of these thin films indicates that the  $Ti_0$  and  $Ti_{0.5}$  alloy thin films have nano-crystalline structures, and  $Ti_1$  alloy thin film has an amorphous structure.



**Figure 3.** TEM BF images and corresponding SAD of as-deposited  $Ti_xFeCoNi$  thin films: (a)  $Ti_0$  film; (b)  $Ti_{0.5}$  film; and (c)  $Ti_{1.0}$  film.

Figure 4 illustrates the structure of stacked layers after annealing is conducted at 1000 °C for 30 min. The variations in the composition along the vertical axis (through thickness) of the layered structures are revealed by the line scan. The compositions at the four selected positions from the surface to the SiO<sub>2</sub> interfacial layer are listed in the inserted tables, and the composition sequences for different films are as follows: (1) Ti<sub>0</sub> film, Fe<sub>6.6</sub>Co<sub>31.6</sub>Ni<sub>0.9</sub>O<sub>60.9</sub> → Fe<sub>26.4</sub>Co<sub>9.8</sub>Ni<sub>1.3</sub>O<sub>62.5</sub> → Fe<sub>2.0</sub>Ni<sub>20.7</sub>Co<sub>74.4</sub>O<sub>2.9</sub> → Fe<sub>26.8</sub>Co<sub>1.7</sub>Si<sub>10.1</sub>O<sub>61.4</sub>; (2) Ti<sub>0.5</sub> film, Ti<sub>0.3</sub>Fe<sub>14.3</sub>Co<sub>13.5</sub>Ni<sub>1.6</sub>Si<sub>0.7</sub>O<sub>69.6</sub> → Fe<sub>15.1</sub>Ni<sub>36.7</sub>Co<sub>40.3</sub>Si<sub>1.1</sub>O<sub>6.8</sub> → Ti<sub>0.1</sub>Fe<sub>7.8</sub>Ni<sub>30.7</sub>Co<sub>54.5</sub>Si<sub>1.2</sub>O<sub>5.7</sub> → Ti<sub>25.8</sub>Fe<sub>2.6</sub>Co<sub>8.9</sub>Ni<sub>2.2</sub>Si<sub>0.6</sub>O<sub>59.9</sub>; and (3) Ti<sub>1.0</sub> film, Ti<sub>0.5</sub>Fe<sub>30.6</sub>Co<sub>11.6</sub>Ni<sub>1.4</sub>Si<sub>0.4</sub>O<sub>55.5</sub> → Ti<sub>39.3</sub>Fe<sub>4.8</sub>Co<sub>0.5</sub>Ni<sub>0.4</sub>Si<sub>1.3</sub>O<sub>53.7</sub> → Ti<sub>0.3</sub>Fe<sub>8.7</sub>Co<sub>35.3</sub>Ni<sub>51.8</sub>Si<sub>0.6</sub>O<sub>3.3</sub> → Ti<sub>45.4</sub>Fe<sub>0.3</sub>Co<sub>0.6</sub>Ni<sub>0.8</sub>Si<sub>0.6</sub>O<sub>52.3</sub>. The oxygen content of the fully-oxidized Me<sub>2</sub>O<sub>3</sub> (60 at % O) and MeO<sub>2</sub> (66.67 at % O) suggests that some of the oxides that form with the residual FeCoNi-rich metal are deficient in oxygen because the oxygen source is insufficient to oxidize the films completely. This oxygen deficiency accounts for the high conductivity of the as-annealed films because more oxygen vacancies can provide more electron carriers to enhance electrical conductivity.



**Figure 4.** Composition distribution of as-annealed Ti<sub>x</sub>FeCoNi thin films, as determined using TEM and EDS: (a) Ti<sub>0</sub>; (b) Ti<sub>0.5</sub>; and (c) Ti<sub>1.0</sub> films.

The layered structure with different phases can be explained from the perspectives of thermodynamics and kinetics. The formation of this structure can be attributed to two factors. (1) Chemical affinity competition or stronger affinity in metal–oxygen pairs, such as SiO and TiO, is preferred to form oxides [6,7]. At 1000 °C, the free energies of the formation follow the increasing order of  $\text{TiO} < \text{SiO} < \text{FeO} < \text{CoO} < \text{NiO}$  (Figure 5); (2) Diffusion rate competition due to the decreasing order of  $\text{O} > \text{Fe} > \text{Co} > \text{Ni} > \text{Ti}$  [8] involves the formation of Fe and Co atoms with high diffusion rates on the top layer, although Ti atoms likely form oxides. The free energies in Figure 5 have been calculated at different temperatures by using Equations (1)–(3) [7]

$$\Delta H_t = \Delta H_0 + 2.303aT \log T + b \times 10^{-3}T^2 + c \times 10^5T^{-1} \quad (1)$$

$$\Delta S_t = -a - 2.303aT \log T - 2b \times 10^{-3}T + c \times 10^5T^{-2} - I \quad (2)$$

$$\Delta F_t = \Delta H - T\Delta S \quad (3)$$

where  $\Delta F_t$  is the free energy of formation,  $\Delta S_t$  is the entropy of formation,  $\Delta H$  is the enthalpy of formation, and  $a$ ,  $b$ , and  $I$  are constants [7].

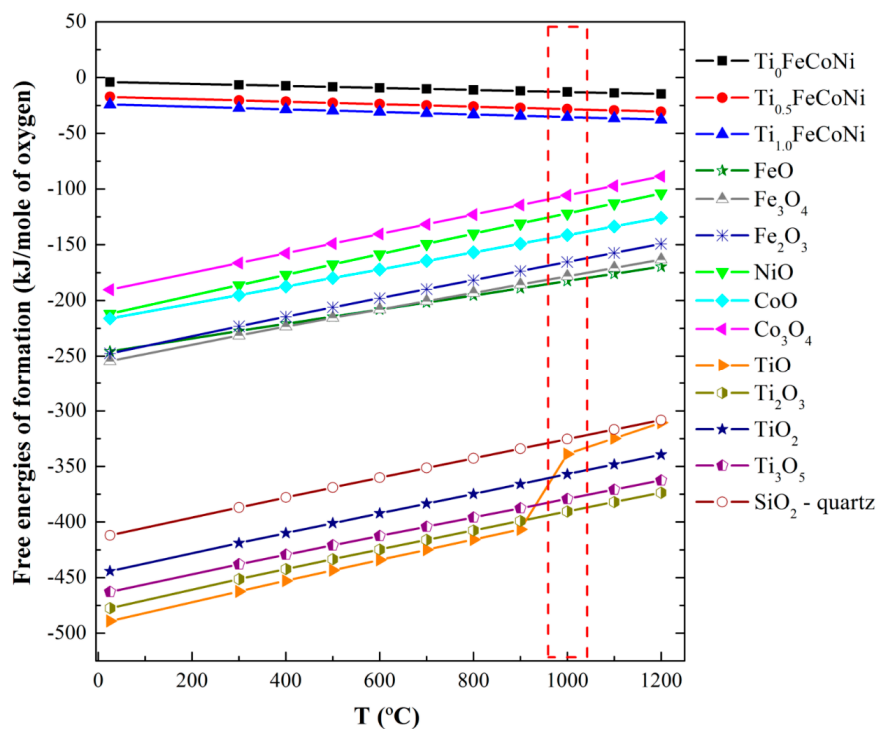


**Figure 5.** Free energies involved in the formation of  $\text{Ti}_x\text{FeCoNi}$  metal and  $\text{A}_n\text{O}_m$  ( $A = \text{Ti, Fe, Co, Ni}$ , and  $\text{Si}$ ) oxides.

Figure 6 presents a schematic of atom migration, diffusion pathways, and reactions during annealing to explain the formation of the layered structure. Figure 6a illustrates the deposition of  $\text{Ti}_x\text{FeCoNi}$  thin films via DC sputtering, resulting in the uniform deposition of constituent atoms on the  $\text{SiO}_2/\text{Si}$  substrate. Figure 6b shows that oxygen transfers from the chamber at a pressure of  $1 \times 10^{-2}$  torr and from the  $\text{SiO}_2/\text{Si}$  substrate under heat treatment at 1000 °C for 30 min. Figure 6c displays the  $\text{Ti}_0$  thin film, in which Fe and Co atoms preferentially react with oxygen to form the top FeCo-rich oxide layer, and with oxygen from the interface layer adjacent to the  $\text{SiO}_2$  to form FeSi-rich oxide layers. Fe–O is even stronger than Co–O. Thus, FeCoNi-rich solid solution phase ( $\text{Ni} > \text{Co} > \text{Fe}$  in concentration) formed as the middle layer. By contrast, the bonding energy of Ti–O is stronger than those of Ti–Fe, Ti–Co, Ti–Ni, Fe–O, Ni–O, and Co–O in the Ti-containing thin film. Figure 6d shows

that this strong affinity causes Ti atoms to migrate into the oxygen-rich region of the thin films during annealing. Thus, the Ti oxide  $Ti_{25.8}Fe_{2.6}Co_{8.9}Ni_{2.2}Si_{0.6}O_{59.9}$  forms near the  $SiO_2$  layer in the  $Ti_{0.5}$  thin film. However, the Ti and Fe contents in the as-deposited  $Ti_{0.5}$  film are 14.3 and 28.6 at %, respectively. The high concentration of Fe (2.6 at %) in Ti oxide suggests that the second-strongest Fe–O bonding can compete with Ti for oxygen when Fe content is relatively high. The FeCoNi-rich metal phase with a large depletion of Ti develops in the middle (see compositions at f and g in Figure 4b). For the  $Ti_{1.0}$  film, in which the Ti content is twice as that of the  $Ti_{0.5}$  film, TiFe-rich oxide is further produced with FeCo-rich oxide on the top layer (at i and j in Figure 4c). In addition, nearly pure Ti oxide with high Ti content but negligible Fe content (0.3 at %) grows with the Ti-depleted and FeCoNi-rich metal phase at the bottom (at k in Figure 4c).

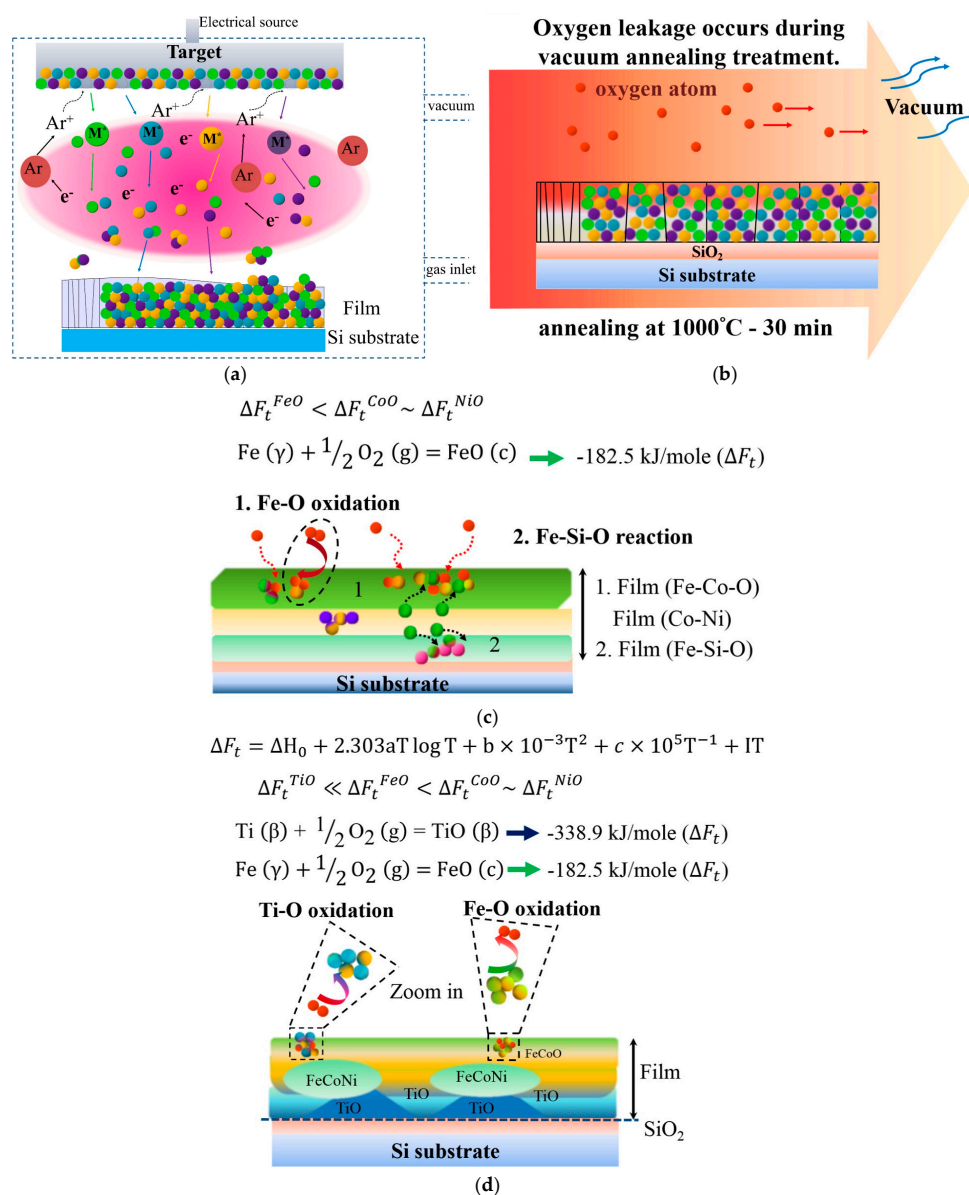


**Figure 6.** Schematic diagram showing the formation of phases in  $Ti_xFeCoNi$  films from the as-deposited state to the post-annealed state: (a) DC sputtering deposition of thin film on Si substrate; (b) oxygen coming from the vacuum chamber and  $SiO_2$  substrate during vacuum annealing; (c) diffusion pathways and layer formation in  $Ti_0$  film during annealing; and (d) diffusion pathways and layer formation in  $Ti_{0.5}$  and  $Ti_{1.0}$  films during annealing.

#### 4. Conclusions

The influence of Ti content and vacuum annealing on the microstructure of  $Ti_xFeCoNi$  thin films was investigated. The as-deposited  $Ti_0$  and  $Ti_{0.5}$  films presented a nano-crystalline FCC structure, while the as-deposited  $Ti_{1.0}$  possessed an X-ray amorphous structure, which can be explained by determining topological instability and by using a hard ball model. The films comprised a layered structure because of phase separation into metal solid solutions and oxygen-deficient oxides after vacuum annealing at 1000 °C for 30 min. Different Ti contents provided various phase separation and layered structures. The mechanism was mainly related to the competition among possible oxides in terms of free energy production at 1000 °C.

**Acknowledgments:** We are grateful to the Ministry of Science and Technology of R.O.C. for the financial support under the project NSC 102-2221-E-007-047-MY3 and MOST 106-2221-E-034-008.

**Author Contributions:** Jien-Wei Yeh and Chun-Huei Tsau conceived and designed the experiments; Ya-Chu Yang performed the experiments; Ya-Chu Yang and Chun-Huei Tsau analyzed the data; Ya-Chu Yang contributed reagents/materials/analysis tools; Ya-Chu Yang wrote the paper. All authors have read and approved the final manuscript.

**Conflicts of Interest:** The authors declare no conflict of interest. The founding sponsors had no role in the design of the study; in the collection, analyses, or interpretation of data; in the writing of the manuscript, or in the decision to publish the results.

#### References

1. Yang, Y.C.; Tsau, C.H.; Yeh, J.W. TiFeCoNi oxide thin film—A new composition with extremely low electrical resistivity at room temperature. *Scr. Mater.* **2011**, *64*, 173–176. [[CrossRef](#)]
2. Tsau, C.H.; Hwang, Z.Y.; Chen, S.K. The microstructures and electrical resistivity of (Al, Cr, Ti)FeCoNiO<sub>x</sub> high-entropy alloy oxide thin films. *Adv. Mater. Sci. Eng.* **2015**, *2015*. [[CrossRef](#)]
3. Callister, W.D., Jr.; Rethwisch, D.G. *Fundamentals of Materials Science and Engineering: An Integrated Approach*, 2nd ed.; John Wiley & Sons, Inc.: Hoboken, NJ, USA, 2005.
4. Kao, S.W.; Yeh, J.W.; Chin, T.S. Rapidly solidified structure of alloys with up to eight equal-molar elements—A simulation by molecular dynamics. *J. Phys. Condens. Matter* **2008**, *20*, 145214. [[CrossRef](#)]
5. Thornton, J.A. High rate thick film growth. *Annu. Rev. Mater. Sci.* **1977**, *7*, 239–260. [[CrossRef](#)]
6. Lynch, C.T. *CRC Handbook of Materials Science: Material Composites and Refractory Materials*; CRC Press: Boca Raton, FL, USA, 1975; Volume 2, pp. 339–352.
7. Pretorius, R.; Harris, J.; Nicolet, M. Reaction of thin metal films with SiO<sub>2</sub> substrates. *Solid-State Electron.* **1978**, *21*, 667–675. [[CrossRef](#)]
8. Koiwa, M. Diffusion in materials—History and recent developments. *Mater. Trans. JIM* **1998**, *39*, 1169–1179. [[CrossRef](#)]



© 2017 by the authors. Licensee MDPI, Basel, Switzerland. This article is an open access article distributed under the terms and conditions of the Creative Commons Attribution (CC BY) license (<http://creativecommons.org/licenses/by/4.0/>).